

# Three new infrared bands of the He - OCS complex

J. Norooz Oliaee,<sup>1</sup> B.L. Brockelbank,<sup>1</sup> A.R.W. McKellar,<sup>2</sup> N. Moazzen-Ahmadi<sup>1\*</sup>

<sup>1</sup> *Department of Physics and Astronomy, University of Calgary, 2500 University Drive North West, Calgary, Alberta T2N 1N4, Canada.*

<sup>2</sup> *National Research Council of Canada, Ottawa, Ontario K1A 0R6, Canada.*

## Abstract

Three new infrared bands of the weakly-bound He-OCS complex are studied, using tunable lasers to probe a pulsed supersonic slit jet expansion. They correspond to the  $(04^0_0) \leftarrow (00^0_0)$ ,  $(10^0_1) \leftarrow (00^0_0)$ , and  $(04^0_1) \leftarrow (00^0_0)$  transitions of OCS at 2105, 2918, and 2937  $\text{cm}^{-1}$ , respectively. The latter band is about 7900 times weaker than the previously studied OCS  $\nu_1$  fundamental. Vibrational shifts relative to the free OCS monomer are found to be additive. Since carbonyl sulfide has previously been shown to be a valuable probe of superfluid quantum solvation effects in helium clusters and droplets, the present results could be useful for future studies of vibrational effects in such systems.

Address for correspondence: Prof. N. Moazzen-Ahmadi,  
Department of Physics and Astronomy,  
University of Calgary,  
2500 University Drive North West,  
Calgary, Alberta T2N 1N4,  
Canada.

\* Corresponding author. Tel: 1-403-220-5394

## 1. Introduction

Intermolecular interactions between He and OCS are of basic interest, but also have taken on practical importance because OCS turns out to be an especially useful probe of microscopic superfluid effects in helium clusters and droplets. This has led to numerous studies of “quantum solvation” in helium probed by OCS, both experimental [1 - 9] and theoretical [11 - 16]. Detailed intermolecular interaction potentials have been calculated for He-OCS, with increasing accuracy over the years [17 - 24]. These potentials can be rigorously tested by comparison with experimental bound-state energy levels of the He-OCS van der Waals complex derived from high-resolution spectra, as observed in the microwave [17, 25] and infrared [26 - 28] regions.

Previous infrared studies of binary He-OCS complexes, and of He<sub>N</sub>-OCS clusters, have been limited to the strong  $\nu_1$  fundamental (C-O stretch) band of OCS located at 2062 cm<sup>-1</sup>. In the present paper, we extend the infrared study of He-OCS to three OCS combination bands at 2105, 2918, and 2937 cm<sup>-1</sup>. Though these transitions are much weaker than  $\nu_1$ , they already provide new information on vibrational shift effects, and could prove useful for future studies of vibrational effects in superfluid helium clusters.

The He-OCS complex has a T-shaped structure, with a binding energy ( $D_0$ ) of about 19 cm<sup>-1</sup> [23], a center of mass separation of about 3.83 Å, and an effective angle of about 66° between the O-C-S molecular axis and the line connecting the centers of mass [6]. It is thus a prolate asymmetric rotor with the  $a$ - and  $b$ -inertial axes approximately aligned with the O-C-S and He-C axes, respectively, and the  $c$ -axis perpendicular to the plane. Since the permanent dipole moment, and stretching transition moments, lie along the O-C-S axis, observed

microwave and infrared transitions are predominately *a*-type ( $\Delta K_a = 0, \Delta K_c = \pm 1$ ) with a weaker *b*-type ( $\Delta K_a = \pm 1, \Delta K_c = \pm 1$ ) contribution .

- **2. Results**

Spectra were recorded at the University of Calgary using a pulsed supersonic slit jet expansion probed by a tunable infrared diode laser (for 2105  $\text{cm}^{-1}$ ) or optical parametric oscillator source (for 2918 and 2937  $\text{cm}^{-1}$ ) as described previously [28-31]. A typical expansion mixture contained 0.1 - 0.2% carbonyl sulfide in helium carrier gas with a jet backing pressure of 10 - 17 atmospheres. Spectral assignment and simulation were made using the PGOPHER software.<sup>32</sup> We label the OCS vibrational states using  $(\nu_1, \nu_2^{l_2}, \nu_3)$ , where  $\nu_1$  represents the C-O stretch,  $\nu_2$  the bend (with angular momentum,  $l_2$ ), and  $\nu_3$  the C-S stretch, with fundamental values of 2062.2, 520.4, and 859.0  $\text{cm}^{-1}$  for  $^{16}\text{O}^{12}\text{C}^{32}\text{S}$ . The He-OCS band in the region of the  $\nu_1$  fundamental band has been studied previously in detail [26 - 28], including some isotopically substituted forms ( $^3\text{He}$ ,  $^{34}\text{S}$ ,  $^{13}\text{C}$ ) in addition to the main isotopologue,  $^4\text{He}-^{16}\text{O}^{12}\text{C}^{32}\text{S}$ .

The OCS combination band  $(04^0_0) \leftarrow (00^0_0)$  is located at 2104.828  $\text{cm}^{-1}$ . This is 42.627  $\text{cm}^{-1}$  above the  $\nu_1$  fundamental band, from which it “steals” some intensity through anharmonic (Fermi) interaction. As a result, the  $(04^0_0) \leftarrow (00^0_0)$  band is much stronger than it would otherwise be, though still about 250 times weaker than  $(10^0_0) \leftarrow (00^0_0)$  [33 - 35]. We have now observed the spectrum of He-OCS in this region, as shown in the top panel of Fig. 1. Rotational analysis of this band was relatively easy, and we assigned a total of 60 transitions with values of  $J'$  and  $K_a'$  up to 6 and 3, respectively. For comparison, in the fundamental band it was possible to observe 133 transitions up to  $(J', K_a') = (8, 4)$  [28].

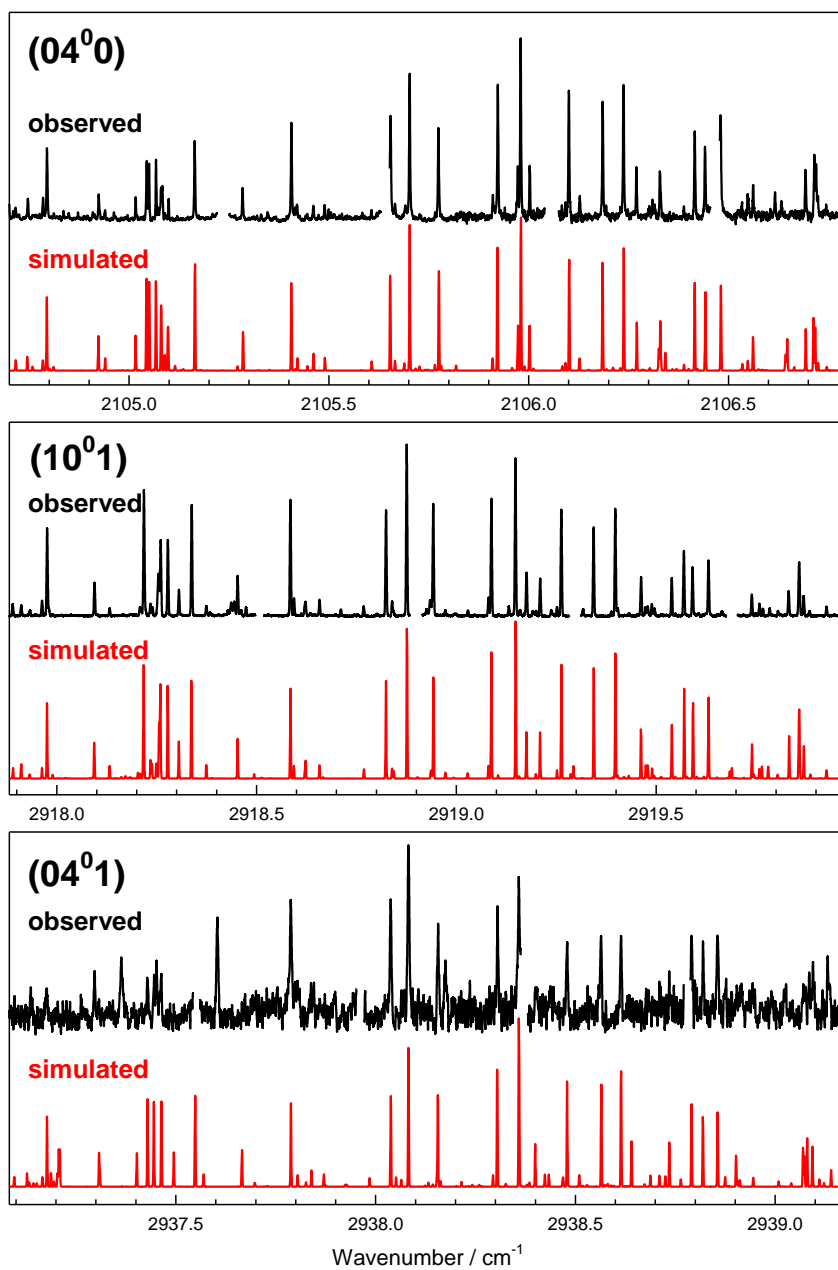


Figure 1. Observed and simulated spectra of He-OCS accompanying three combination bands of OCS. Gaps in the experimental traces are regions obscured by OCS monomer transitions.

Table 1. Molecular parameters for He - OCS complexes (in  $\text{cm}^{-1}$ ).<sup>a</sup>

	(00 <sup>0</sup> 0)	(10 <sup>0</sup> 0)	(04 <sup>0</sup> 0)	(10 <sup>0</sup> 1)	(04 <sup>0</sup> 1)
$\nu_0$		2062.3125(2)	2105.0997(4)	2918.2810(3)	2937.4832(4)
$\Delta\nu_0$		+0.1117	+0.2720	+0.1761	+0.3364
$A$	0.440779(3)	0.43622(15)	0.45326(68)	0.43818(21)	0.45134(54)
$B$	0.18337(4)	0.18304(9)	0.18731(14)	0.182562(48)	0.18120(26)
$C$	0.12236(4)	0.12136(9)	0.11928(15)	0.121066(38)	0.12326(26)
$10^3 \times \Delta_K$	1.694(5)	0.94(3)	10.47(20)	1.680(35)	5.40(11)
$10^5 \times \Delta_{JK}$	3.97(18)	5.6(12)	10.5(66)	2.98(104)	45.0(62)
$10^5 \times \Delta_J$	3.105(11)	2.97(9)	9.65(23)	3.247(60)	-2.79(86)
$10^4 \times \delta_K$	1.96(21)	4.3(5)	16.31(49)	4.36(12)	-3.6(13)
$10^5 \times \delta_J$	1.086(3)	1.07(7)	3.24(10)	1.244(34)	
$10^4 \times H_K$	0.270(15)	-1.8(3)	7.91(12)	0.400(15)	
$10^5 \times H_{KJ}$	2.05(13)	0.5(3)	4.99(99)	0.397(97)	
$10^5 \times H_{JK}$	-0.35(3)	0.07(8)	0.56(13)		
$10^7 \times H_J$	-0.25(4)	-0.37(12)			
$10^5 \times h_K$	-1.9(3)	1.5(7)		1.42(12)	
$10^7 \times h_J$	-0.46(3)	-0.21(11)			
rms error		0.0008	0.00085	0.00068	0.00057

<sup>a</sup> Uncertainties in parentheses are  $1\sigma$  from the least-squares fits, expressed in units of the last quoted digit. The (00<sup>0</sup>0) and (10<sup>0</sup>0) parameters are from [28]; remaining parameters are the current work.

The  $\nu_1 + \nu_3$  combination band of OCS, located at  $2918.105 \text{ cm}^{-1}$ , is about 70 times weaker than  $\nu_1$ , which makes it about 3.5 times stronger than the  $4\nu_2$  band just described. Our observed spectrum of He-OCS in this region is shown in the middle panel of Fig. 1. Here, we assigned 114 transitions up to  $(J', K_a') = (8, 4)$ .

Just as the  $(04^00)$  state steals intensity from  $(10^00)$ , so  $(04^01)$  also steals from  $(10^01)$ . However, in the latter case the separation of the two states is only  $19 \text{ cm}^{-1}$  (as compared to  $43 \text{ cm}^{-1}$ ), so the interaction is somewhat stronger, and the  $(04^01) \leftarrow (00^00)$  band turns out to be about 110 times weaker than  $(10^01) \leftarrow (00^00)$ , and hence about 7900 times weaker than  $\nu_1$  [33]. Our observed spectrum of He-OCS in this region is shown in the bottom panel of Fig. 1. It is immediately evident that the signal to noise ratio in this spectrum is much worse than the others, which is not surprising given the weakness of the OCS band. Detection of this band was possible by implementation of quantum-correlated twin beams (idler and signal) for cancellation of the power fluctuations in the rapid-scan mode [36]. Even so, we were able to assign 23 transitions up to  $(J', K_a') = (5, 2)$  and these assignments were virtually unambiguous, thanks to the relatively simple and widely-spaced nature of the He-OCS spectrum.

We fitted the observed transitions using the Watson *A*-reduced Hamiltonian with results as shown in Table 1. Ground state parameters were fixed at those determined previously [28] using microwave [17, 25] and  $\nu_1$  fundamental band [28] data. The table includes these ground and  $\nu_1$  state parameters, for comparison with the new results. Complete lists of observed and calculated line positions are given in Tables A1-A3. The root mean square errors of the fits were  $0.00085$ ,  $0.00068$ , and  $0.00057 \text{ cm}^{-1}$  for the three new bands,  $(04^00)$ ,  $(10^01)$ , and  $(04^01)$ , respectively. These values are similar to that achieved for the  $\nu_1$  fundamental [28], but larger

than the estimated relative experimental accuracy which is about 0.0002 to 0.0003  $\text{cm}^{-1}$ . This may be a reflection of the inadequacy of a conventional (semi-rigid molecule) Hamiltonian to fit the rotational levels of a floppy and weakly-bound complex such as He-OCS, in spite of including many centrifugal distortion parameters. Similarly, note that the ratios of the number of fitted (upper state) levels to the number of varied parameters were relatively small: 28/13, 49/13, and 18/9 for the three bands. For these reasons, one should be cautious about the significance of the parameters in Table 1 (especially the higher-order ones) and be aware that their quoted standard deviations likely underestimate the true uncertainties.

- **3. Discussion and conclusions**

It is interesting to consider the He-OCS band origins in terms of their shift,  $\Delta\nu_0$ , relative to the free OCS molecule, as summarized near the top of Table 1. In all cases, there is a small positive (“blue”) shift (0.11 to 0.34  $\text{cm}^{-1}$ ), indicating that the van der Waals bond becomes slightly weaker in the excited vibrational states. The shifts observed here for the combination bands are larger than that of the  $\nu_1$  fundamental. Most notable is the fact that the shift for the (04<sup>0</sup>1) upper state is exactly equal (within experimental error) to the sum of the shifts for (04<sup>0</sup>0) and (10<sup>0</sup>1) minus the shift for (10<sup>0</sup>0). This is just what one would expect if the shifts were simple additive functions of the OCS vibrational quantum numbers. In this context, it would be interesting to measure the He-OCS shift for the OCS  $\nu_3$  fundamental band at 859  $\text{cm}^{-1}$ , which should be equal to +0.0644  $\text{cm}^{-1}$  if this trend continued.

Experimental line widths in the current spectra ( $\approx 0.003 \text{ cm}^{-1}$ ) were limited by residual Doppler broadening due to the (multi-passed) laser beam not being perfectly orthogonal to the velocities of the molecules in the supersonic expansion. There was no evidence of further

broadening due to predissociation, that is, due to finite upper state lifetimes. The present results show that it is now possible to detect spectra of weakly-bound complexes even for fairly weak infrared bands. In particular, the current result for the  $(04^0_1) \leftarrow (00^0_0)$  band of OCS (transition dipole moment  $\approx 0.0036$  Debye [33]) probably represents the weakest of many such bands studied using our apparatus over the past ten years.

### **Acknowledgments**

Financial support from the Natural Sciences and Engineering Research Council of Canada is gratefully acknowledged. We thank A.J. Barclay and K. Esteki for assistance with the experiment.

### **Appendix A. Supplementary material**

Supplementary data associated with this article can be found, in the online version at <http://dx.doi.org/10.1016/j.jms.2017.xx.xxx>.



## References

- [1] S. Grebenev, M. Hartmann, M. Havenith, B. Sartakov, J.P. Toennies, A.F. Vilesov, J. Chem. Phys. 112 (2000) 4485.
- [2] S. Grebenev, J.P. Toennies, A.F. Vilesov, Science 279 (1998) 2083.
- [3] S. Grebenev, M. Havenith, F. Madeja, J.P. Toennies, A.F. Vilesov, J. Chem. Phys. 113 (2000) 9060.
- [4] M. Kunze, P.R.L. Marwick, N. Pörtner, J. Reuss, M. Havenith, J. Chem. Phys. 116 (2002) 7473.
- [5] J. Tang, Y. Xu, A.R.W. McKellar, W. Jäger, Science 297 (2002) 2030.
- [6] J. Tang, A.R.W. McKellar, J. Chem. Phys. 119 (2003) 5467.
- [7] Y. Xu, W. Jäger, J. Chem. Phys. 119 (2003) 5457.
- [8] A.R.W. McKellar, Y. Xu, W. Jäger, Phys. Rev. Lett. 97 (2006) 183401.
- [9] A.R.W. McKellar, Y. Xu, W. Jäger, J. Phys. Chem. A 111 (2007) 7329.
- [10] B.G. Sartakov, J.P. Toennies, A.F. Vilesov, J. Chem. Phys. 136 (2012) 134316.
- [11] Y. Kwon, K.B. Whaley, J. Chem. Phys. 115 (2001) 10146.
- [12] F. Paesani, F.A. Gianturco, K.B. Whaley, J. Chem. Phys. 115 (2001) 10225.
- [13] S. Moroni, A. Sarsa, S. Fantoni, K.E. Schmidt, S. Baroni, Phys. Rev. Lett. 90 (2003) 143401.
- [14] F. Paesani, A. Viel, F.A. Gianturco, K.B. Whaley, Phys. Rev. Lett. 90 (2003) 073401.
- [15] S. Paolini, S. Fantoni, S. Moroni, S. Baroni, J. Chem. Phys. 123 (2005) 114306.
- [16] S. Miura, J. Chem. Phys. 126 (2007) 114309.
- [17] K. Higgins, W. Klemperer, J. Chem. Phys. 110 (1999) 1383.
- [18] M. Keil, L. Rawluck, T.W. Dingle, J. Chem. Phys. 96 (1992) 6621.
- [19] J. Sadlej, D. Edwards, Int. J. Quantum Chem. 46 (1993) 623.
- [20] J.M.M. Howson, J. Hutson, J. Chem. Phys. 115 (2001) 5059.

- [21] F. A. Gianturco, F. Paesani, *J. Chem. Phys.* 113 (2000) 3011.
- [22] F. Paesani, K.B. Whaley, *J. Chem. Phys.* 121 (2004) 4180.
- [23] H. Li, Y.-T. Ma, *J. Chem. Phys.* 137 (2012) 234310.
- [24] Z. Wang, E. Feng, C. Zhang, C. Sun, *J. Chem. Phys.* 141 (2014) 174308.
- [25] Y. Xu, W. Jäger, *J. Mol. Spectrosc.* 251 (2008) 326.
- [26] J. Tang, A.R.W. McKellar, *J. Chem. Phys.* 115 (2001) 3053.
- [27] J. Tang, A.R.W. McKellar, *J. Chem. Phys.* 117 (2002) 2586.
- [28] Z. Abusara, L. Borvayeh, N. Moazzen-Ahmadi, A.R.W. McKellar, *J. Chem. Phys.* 125 (2006) 144306.
- [29] M. Dehghany, M. Afshari, Z. Abusara, C. Van Eck, N. Moazzen-Ahmadi, *J. Mol. Spectrosc.* 247 (2008) 123.
- [30] M. Rezaei, K.H. Michaelian, N. Moazzen-Ahmadi, *J. Chem. Phys.* 136 (2012) 124308.
- [31] M. Rezaei, S. Sheybani-Deloui, N. Moazzen-Ahmadi, K.H. Michaelian, A.R.W. McKellar, *J. Phys. Chem. A* 117 (2013) 9612.
- [32] C.M. Western, PGOPHER, a program for simulating rotational structure version 8.0, 2014, University of Bristol Research Data Repository, [doi:10.5523/bris.huflggvpcuc1zvliqed497r2](https://doi.org/10.5523/bris.huflggvpcuc1zvliqed497r2)
- [33] A.G. Maki, J.S. Wells, "Wavenumber calibration tables from heterodyne frequency measurements," NIST Special Publication 821, U.S. Government Printing Office, 1991.
- [34] A. Foord, A.G. Whiffen, *Mol. Phys.* 26 (1973) 959.
- [35] N. Hunt, S.C. Foster, J.W.C. Johns, A.R.W. McKellar, *J. Mol. Spectrosc.* 111 (1985) 42.
- [36] J. Norooz Oliaee, B. Brockelbank, N. Moazzen-Ahmadi, "Use of quantum-correlated twin beams for cancellation of power fluctuations in a continuous-wave optical parametric oscillator for high-resolution spectroscopy in the rapid scan," The 25<sup>th</sup> Colloquium on High Resolution Molecular Spectroscopy, 20-25 August, Helsinki, Finland (2017).

## Appendix A

Table A1. Observed and calculated transitions in the (0400)  $\leftarrow$  (0000), band of He-OCS dimer around 2105  $\text{cm}^{-1}$  (units of  $\text{cm}^{-1}$ ).

```

*****
J'   Ka'  Kc'   J''  Ka'' Kc''  Observed  Calculated  Obs-Calc
*****
0     0    0     1    0   1   2104.79448 2104.79406   0.00041
0     0    0     1    1   1   2104.53816 2104.53790   0.00025
1     1    0     2    1   1   2104.43374 2104.43479  -0.00105
1     1    0     1    1   1   2105.16416 2105.16492  -0.00076
1     1    0     1    0   1   2105.42031 2105.42108  -0.00077
1     0    1     2    0   2   2104.49886 2104.49887  -0.00001
1     0    1     0    0   0   2105.40609 2105.40587   0.00021
1     0    1     1    1   0   2104.78455 2104.78404   0.00050
1     1    1     2    1   2   2104.55316 2104.55320  -0.00004
1     1    1     1    1   0   2105.04400 2105.04362   0.00037
1     1    1     0    0   0   2105.66549 2105.66545   0.00003
2     0    2     1    0   1   2105.70206 2105.70231  -0.00025
2     0    2     2    1   1   2104.71582 2104.71602  -0.00020
2     1    2     1    0   1   2105.91034 2105.90944   0.00089
2     1    2     2    1   1   2104.92392 2104.92314   0.00077
2     1    2     3    1   3   2104.28394 2104.28296   0.00097
2     1    2     1    1   1   2105.65414 2105.65327   0.00086
2     2    0     1    1   1   2106.54866 2106.54829   0.00036
2     2    0     2    2   1   2105.06737 2105.06721   0.00015
2     1    1     1    1   0   2105.77418 2105.77538  -0.00120
2     1    1     2    1   2   2105.28401 2105.28496  -0.00095
2     1    1     2    0   2   2105.48915 2105.49020  -0.00105
2     2    1     2    2   0   2105.04995 2105.05009  -0.00014
3     1    2     3    0   3   2105.60652 2105.60714  -0.00062
3     1    2     2    1   1   2106.10054 2106.10155  -0.00101
3     1    2     3    1   3   2105.46111 2105.46137  -0.00026
3     2    2     3    2   1   2105.01643 2105.01635   0.00007
3     2    2     2    2   1   2105.97275 2105.97321  -0.00046
3     2    2     3    1   3   2106.08291 2106.08399  -0.00108
3     3    0     2    2   1   2107.35775 2107.35732   0.00042
3     3    0     3    3   1   2105.08090 2105.08102  -0.00012
3     0    3     2    0   2   2105.97987 2105.98038  -0.00051
3     0    3     3    1   2   2104.59845 2104.59849  -0.00004
3     1    3     3    1   2   2104.74660 2104.74520   0.00139
3     1    3     2    1   2   2105.92271 2105.92185   0.00085
3     1    3     2    0   2   2106.12784 2106.12709   0.00074
3     2    1     2    2   0   2106.00260 2106.00208   0.00051
3     2    1     3    1   2   2105.76595 2105.76509   0.00085
3     2    1     3    2   2   2105.09890 2105.09784   0.00105
3     3    1     3    3   0   2105.08050 2105.07991   0.00058
3     3    1     2    2   0   2107.34707 2107.34794  -0.00087
4     0    4     3    1   3   2106.09208 2106.09218  -0.00010
4     0    4     3    0   3   2106.23729 2106.23796  -0.00067
4     1    4     3    1   3   2106.18511 2106.18506   0.00004

```

4	2	2	3	2	1	2106.32845	2106.32952	-0.00107
4	2	2	4	2	3	2105.16416	2105.16430	-0.00014
4	1	3	3	1	2	2106.41556	2106.41529	0.00026
4	1	3	4	1	4	2105.69117	2105.68869	0.00247
4	2	3	4	2	2	2104.93971	2104.94026	-0.00055
4	2	3	3	2	2	2106.26965	2106.27036	-0.00071
5	1	4	4	1	3	2106.71492	2106.71285	0.00206
5	2	4	4	2	3	2106.56175	2106.56133	0.00041
5	2	4	5	2	3	2104.81167	2104.81105	0.00061
5	0	5	4	0	4	2106.47992	2106.48103	-0.00111
5	0	5	4	1	4	2106.38836	2106.38885	-0.00049
5	1	5	4	1	4	2106.44136	2106.44243	-0.00107
5	1	5	4	0	4	2106.53355	2106.53462	-0.00107
6	0	6	5	0	5	2106.71940	2106.71724	0.00215
6	1	6	5	1	5	2106.69284	2106.69322	-0.00038
6	1	5	5	1	4	2106.99152	2106.99296	-0.00144

Table A2. Observed and calculated transitions in the (1001)  $\leftarrow$  (0000) band of He-OCS dimer around 2918  $\text{cm}^{-1}$  (units of  $\text{cm}^{-1}$ ).

```

*****
  J'   Ka'  Kc'   J''  Ka'' Kc''  Observed  Calculated  Obs-Calc
*****
  0     0    0     1    1    1   2917.71910  2917.71921  -0.00010
  0     0    0     1    0    1   2917.97583  2917.97537   0.00045
  1     1    0     1    0    1   2918.59374  2918.59340   0.00033
  1     1    0     2    1    1   2917.60706  2917.60711  -0.00004
  1     0    1     1    1    0   2917.96310  2917.96264   0.00045
  1     0    1     2    1    2   2917.47183  2917.47223  -0.00039
  1     0    1     2    0    2   2917.67729  2917.67747  -0.00017
  1     0    1     0    0    0   2918.58467  2918.58448   0.00019
  1     1    1     1    1    0   2918.21812  2918.21746   0.00065
  1     1    1     2    2    0   2916.78766  2916.78737   0.00028
  1     1    1     2    0    2   2917.93286  2917.93228   0.00057
  1     1    1     2    1    2   2917.72709  2917.72704   0.00004
  2     0    2     1    0    1   2918.87574  2918.87610  -0.00036
  2     0    2     2    1    1   2917.88962  2917.88981  -0.00019
  2     0    2     3    0    3   2917.39503  2917.39540  -0.00037
  2     1    2     1    1    1   2918.82403  2918.82422  -0.00018
  2     1    2     3    1    3   2917.45382  2917.45391  -0.00009
  2     1    2     2    1    1   2918.09445  2918.09409   0.00035
  2     1    2     3    0    3   2917.59947  2917.59969  -0.00022
  2     1    2     1    0    1   2919.08050  2919.08039   0.00011
  2     2    0     1    1    1   2919.75876  2919.75870   0.00005
  2     2    0     3    2    1   2917.32048  2917.32075  -0.00027
  2     2    0     2    1    1   2919.02887  2919.02858   0.00029
  2     2    0     2    2    1   2918.27799  2918.27761   0.00037
  2     1    1     2    0    2   2918.65758  2918.65752   0.00005
  2     1    1     2    1    2   2918.45258  2918.45228   0.00030
  2     1    1     3    1    2   2917.27559  2917.27563  -0.00004
  2     1    1     2    2    0   2917.51253  2917.51261  -0.00008
  2     1    1     1    1    0   2918.94218  2918.94270  -0.00051
  2     2    1     2    2    0   2918.25998  2918.25957   0.00040
  2     2    1     3    2    2   2917.35511  2917.35533  -0.00021
  3     1    2     4    1    3   2916.95253  2916.95237   0.00016
  3     1    2     3    2    1   2917.55427  2917.55487  -0.00060
  3     1    2     2    1    1   2919.26270  2919.26269   0.00000
  3     1    2     3    0    3   2918.76811  2918.76829  -0.00017
  3     1    2     3    1    3   2918.62202  2918.62251  -0.00049
  3     2    2     2    2    1   2919.17568  2919.17567   0.00000
  3     2    2     4    2    3   2917.05344  2917.05358  -0.00014
  3     2    2     3    2    1   2918.21812  2918.21881  -0.00069
  3     2    2     2    1    1   2919.92639  2919.92663  -0.00024
  3     3    0     4    3    1   2917.02094  2917.01979   0.00114
  3     3    0     2    2    1   2920.53148  2920.53173  -0.00024
  3     0    3     4    1    4   2917.03959  2917.03940   0.00018
  3     0    3     4    0    4   2917.13138  2917.13158  -0.00019
  3     0    3     3    1    2   2917.76597  2917.76600  -0.00003
  3     0    3     2    0    2   2919.14787  2919.14789  -0.00002

```

3	1	3	3	1	2	2917.91109	2917.91124	-0.00014
3	1	3	4	1	4	2917.18463	2917.18463	-0.00000
3	1	3	2	1	2	2919.08776	2919.08789	-0.00012
3	2	1	3	2	2	2918.30569	2918.30554	0.00015
3	2	1	2	0	2	2920.35486	2920.35469	0.00016
3	2	1	2	1	2	2920.14927	2920.14945	-0.00017
3	2	1	3	1	2	2918.97246	2918.97280	-0.00033
3	2	1	2	2	0	2919.20982	2919.20978	0.00003
3	2	1	4	2	2	2916.97513	2916.97543	-0.00030
3	3	1	2	2	0	2920.52174	2920.52184	-0.00009
3	3	1	4	3	2	2917.02619	2917.02432	0.00186
4	0	4	3	1	3	2919.25196	2919.25196	0.00000
4	0	4	3	0	3	2919.39775	2919.39773	0.00001
4	0	4	4	1	3	2917.58139	2917.58181	-0.00041
4	1	4	3	1	3	2919.34350	2919.34387	-0.00036
4	1	4	3	0	3	2919.48922	2919.48964	-0.00042
4	1	4	5	1	5	2916.91980	2916.91933	0.00046
4	2	2	4	2	3	2918.37430	2918.37389	0.00041
4	2	2	3	1	3	2920.60720	2920.60675	0.00044
4	2	2	5	2	3	2916.62354	2916.62361	-0.00007
4	2	2	3	2	1	2919.53903	2919.53911	-0.00007
4	3	2	3	3	1	2919.47374	2919.47497	-0.00123
4	3	2	4	3	1	2918.23955	2918.23933	0.00021
4	3	2	3	2	1	2920.79294	2920.79441	-0.00146
4	4	0	4	4	1	2918.23442	2918.23447	-0.00005
4	1	3	5	1	4	2916.64257	2916.64199	0.00057
4	1	3	4	0	4	2918.93435	2918.93518	-0.00082
4	1	3	3	1	2	2919.56938	2919.56959	-0.00021
4	2	3	5	2	4	2916.75684	2916.75671	0.00012
4	2	3	3	2	2	2919.46236	2919.46250	-0.00013
4	2	3	3	1	2	2920.12934	2920.12976	-0.00041
4	2	3	4	2	2	2918.13223	2918.13239	-0.00016
4	3	1	3	3	0	2919.47886	2919.47979	-0.00092
4	4	1	4	4	0	2918.23442	2918.23437	0.00004
5	1	4	4	1	3	2919.85793	2919.85866	-0.00073
5	1	4	6	1	5	2916.35100	2916.34924	0.00176
5	2	4	4	2	3	2919.73941	2919.73956	-0.00014
5	3	2	5	3	3	2918.25463	2918.25415	0.00047
5	3	2	4	3	1	2919.78420	2919.78328	0.00092
5	3	2	4	2	3	2921.17306	2921.17313	-0.00007
5	0	5	6	0	6	2916.63318	2916.63291	0.00027
5	0	5	4	0	4	2919.63102	2919.63150	-0.00048
5	1	5	4	1	4	2919.59111	2919.59195	-0.00084
5	1	5	6	1	6	2916.65823	2916.65729	0.00093
5	2	3	6	2	4	2916.27750	2916.27659	0.00091
5	2	3	4	2	2	2919.86917	2919.86908	0.00009
5	3	3	4	2	2	2921.02800	2921.03048	-0.00247
5	3	3	4	3	2	2919.76732	2919.76730	0.00002
6	0	6	7	0	7	2916.38537	2916.38382	0.00155
6	0	6	5	0	5	2919.85793	2919.85775	0.00018
6	1	6	5	1	5	2919.83159	2919.83265	-0.00106
6	1	6	7	1	7	2916.39960	2916.39727	0.00233

6	1	6	5	0	5	2919.88394	2919.88556	-0.00161
6	2	4	5	2	3	2920.18867	2920.18846	0.00020
6	3	4	5	3	3	2920.05376	2920.05302	0.00073
6	1	5	5	1	4	2920.12534	2920.12545	-0.00010
6	2	5	5	2	4	2920.00599	2920.00574	0.00025
6	3	3	5	3	2	2920.09400	2920.09212	0.00188
7	1	6	6	1	5	2920.36824	2920.36807	0.00017
7	2	6	6	2	5	2920.26151	2920.26090	0.00060
7	3	4	6	3	3	2920.40870	2920.40792	0.00077
7	0	7	6	1	6	2920.05376	2920.05310	0.00065
7	1	7	6	1	6	2920.06592	2920.06672	-0.00080
7	2	5	6	2	4	2920.48824	2920.48998	-0.00173
7	3	5	6	3	4	2920.32950	2920.33080	-0.00129
8	0	8	7	0	7	2920.30258	2920.30307	-0.00048
8	1	7	7	1	6	2920.59034	2920.59011	0.00022
8	2	7	7	2	6	2920.50625	2920.50625	0.00000

Table A3. Observed and calculated transitions in the (0401)  $\leftarrow$  (0000) band of He-OCS dimer around 2938  $\text{cm}^{-1}$  (units of  $\text{cm}^{-1}$ ).

```

*****
  J'   Ka'  Kc'   J''  Ka'' Kc''  Observed  Calculated  Obs-Calc
*****
  0     0    0     1    0    1   2937.17651  2937.17754  -0.00102
  1     1    0     2    1    1   2936.81893  2936.81832   0.00061
  1     0    1     0    0    0   2937.78770  2937.78772  -0.00002
  1     0    1     2    0    2   2936.88066  2936.88072  -0.00005
  1     1    1     2    1    2   2936.93922  2936.93859   0.00062
  1     1    1     1    1    0   2937.42894  2937.42901  -0.00006
  2     0    2     1    0    1   2938.08216  2938.08194   0.00022
  2     0    2     3    0    3   2936.60214  2936.60124   0.00089
  2     1    2     1    1    1   2938.03759  2938.03772  -0.00013
  2     1    2     2    1    1   2937.30659  2937.30759  -0.00100
  2     1    2     3    1    3   2936.66705  2936.66741  -0.00035
  2     2    0     2    2    1   2937.46284  2937.46386  -0.00101
  2     1    1     1    1    0   2938.15625  2938.15578   0.00046
  2     2    1     2    2    0   2937.44570  2937.44479   0.00090
  3     1    2     2    1    1   2938.47898  2938.47940  -0.00041
  3     0    3     2    0    2   2938.35840  2938.35818   0.00022
  3     1    3     2    1    2   2938.30508  2938.30434   0.00073
  4     0    4     3    0    3   2938.61401  2938.61420  -0.00019
  4     1    4     3    1    3   2938.56394  2938.56460  -0.00065
  4     2    2     3    2    1   2938.73482  2938.73470   0.00011
  4     1    3     3    1    2   2938.79062  2938.79075  -0.00013
  5     0    5     4    0    4   2938.85581  2938.85592  -0.00010
  5     1    5     4    1    4   2938.81945  2938.81905   0.00040
*****

```